Received: 24 December 2019 | Revised: 1 March 2020 | Accepted: 11 March 2020 | Published online: 29 April 2020

DOI: 10.1002/dad2.12030

Alzheimer's & Dementia
Diagnosis, Assessment & Disease Monitoring

NEUROIMAGING

Intrathecal ^{99m}Tc-DTPA imaging of molecular passage from lumbar cerebrospinal fluid to brain and periphery in humans

Ajay Verma[1] | **Jacob Y. Hesterman**[2] | **J. Levi Chazen**[3] | **Robert Holt**[2] | **Patrick Connolly**[2] | **Laura Horky**[4] | **Shankar Vallabhajosula**[3] | **P. David Mozley**[3]

[1]Codiak Biosciences, Cambridge, Massachusetts

[2]inviCRO, Boston, Massachusetts

[3]Cornell University Weill College of Medicine, New York, New York

[4]Kaiser Permanente, San Diego, California

Correspondence
Ajay Verma, Codiak Biosciences, Cambridge, MA, USA
Email: ajay.verma@codiakbio.com

Abstract

Introduction: Cerebrospinal fluid (CSF) molecular exchange with brain interstitial fluid (ISF) and periphery is implicated in neurological disorders but needs better quantitative clinical assessment approaches.

Methods: Following intrathecal (ITH) dosing via lumbar puncture, Technetium-99 m (^{99m}Tc-) diethylenetriaminepentaacetic acid (DTPA) imaging was used to quantify neuraxial spread, CSF-brain molecular exchange, and CSF-peripheral clearance in 15 normal human volunteers. The effect of experimental convection manipulation on these processes was also assessed.

Results: Rostral cranial ^{99m}Tc-DTPA exposures were influenced by the volume of artificial CSF in the formulation. Signal translocation to the cranial cisterns and the brain parenchyma was observable by 3 hours. ^{99m}Tc-DTPA penetrated cortical ISF but showed lower signal in deeper structures. Urinary ^{99m}Tc-DTPA signal elimination was accelerated by higher formulation volumes and mechanical convection.

Discussion: Widely used for detecting CSF leaks, ITH ^{99m}Tc-DTPA imaging can also become a useful clinical biomarker for measuring molecular exchange physiology between the CSF, brain, and periphery.

KEYWORDS

brain clearance, cerebrospinal fluid, imaging, biomarker, intrathecal

1 | INTRODUCTION

The intrathecal (ITH) dosing route, whereby molecules are delivered directly across the dura mater of the meninges into the cerebrospinal fluid (CSF) within the subarachnoid space (SAS), allows bypassing of the blood-brain barrier (BBB) to access the central nervous system (CNS) more directly. Although increasingly utilized for clinical drug delivery, use of ITH dosing for allowing CNS access to biomarker imaging probes remains largely unexploited. Many imaging probes already in widespread clinical practice, which do not cross the BBB, could be administered intrathecally for evaluating a spectrum of CNS physiological processes. Possible applications for ITH molecular imaging include quantification of CNS target concentrations, energy metabolism, inflammation, CSF fluid dynamics, and CSF-brain molecular exchange. To develop such clinical ITH molecular imaging approaches, several anatomical, physiological, molecular, dosing, and dosimetry features influencing clinical implementation need to be evaluated. We have shown that in vivo human CSF volumes estimated

This is an open access article under the terms of the Creative Commons Attribution-NonCommercial-NoDerivs License, which permits use and distribution in any medium, provided the original work is properly cited, the use is non-commercial and no modifications or adaptations are made.
© 2020 The Authors. *Alzheimer's & Dementia: Diagnosis, Assessment & Disease Monitoring* published by Wiley Periodicals, Inc. on behalf of the Alzheimer's Association.

with advanced magnetic resonance imaging (MRI) techniques are substantially higher than those previously reported in the literature.[1] Neuraxial CSF movement can also be influenced by convective forces resulting from breathing and heart contraction mechanics[2] and from the bolus volumes used for ITH dosing,[3-5] and we have evaluated such factors in this study to develop ^{99m}Tc-diethylenetriaminepentaacetic acid (DTPA) ITH imaging as a biomarker for exchange processes between the CSF, CNS, and periphery.

The recent resurgence of interest in CSF-brain molecular exchange mechanisms and CSF clearance routes to the periphery stems from animal experiments and human observations, which suggest an important role for these processes in the removal of metabolic waste and aggregation-prone proteins from the brain as well as in CNS immune surveillance processes.[6,7] Deficiencies in these processes have been proposed to contribute to the development of several aging-related, inflammatory, and traumatic diseases including Alzheimer's dementia, multiple sclerosis, and chronic traumatic encephalopathy.[6-10] However, reliable clinical measurement tools are needed to enable clinical research toward disease-related monitoring and therapeutic manipulation of these processes. Attempts to clinically study in vivo CSF-brain molecular exchange activity, or the "glymphatic system," as it is more recently referred to,[8,9,11,12] have so far relied on ITH dosing and imaging of MR susceptibility probes such as Gd-DTPA. Metal chelates of DTPA do not cross the intact BBB but are known to enter the brain interstitial space from the CSF.[2] The ability of Gd-DTPA and other Gd-containing probes to penetrate brain cortical parenchyma over time following ITH dosing into the CSF has been demonstrated in multiple mammalian species including humans.[12-15] However, the millimolar amount of Gd required for MRI visualization gives poor resolution of the lower Gd-DTPA concentrations that penetrate CNS tissue after ITH dosing, thus providing an incomplete and non-quantitative view of this biology. The clinical safety of ITH Gd administration and appropriate dose is also currently under debate, since demetallation of Gd-DTPA complexes can occur in vivo with potentially toxic accumulation of Gd in CNS cells over time.[16]

By contrast, quantitative ITH imaging with positron emission tomography (PET) and single photon emission tomography (SPECT) radioisotopes requires nanomolar to picomolar doses of probes. ^{111}In-DTPA and ^{99m}Tc-DTPA are in fact routinely used clinically to assess CSF leaks from the ITH space following their lumbar cistern dosing.[17] The high stability of the ^{99m}Tc-DTPA complex, its 6-hour physical half-life, and acceptable ITH CNS radiation absorbed dose[18] make it useful for imaging procedures lasting 24 hours. This period is well suited for quantifying the relatively slow ITH molecular kinetics. In extending the use of clinical ITH ^{99m}Tc-DTPA imaging to explore molecular pharmacokinetics, we first evaluate the impact of several parameters on cranial delivery of ^{99m}Tc-DTPA, including lumbar dosing volumes and mechanical forces. Then, using SPECT/CT with attenuation correction, we evaluate the movement of ^{99m}Tc-DTPA from the cranial SAS into brain tissue. We also capitalize on the intact and exclusive renal excretion of ^{99m}Tc-DTPA without any in vivo metabolism to track its peripheral CSF outflow pathway (PCOP) mediated clearance[19,20] and urinary excretion of ^{99m}Tc-DTPA.

RESEARCH IN CONTEXT

1. Systemic review: Recent interest in the exchange of molecules from the brain to cerebrospinal fluid (CSF) as well as molecular clearance from the neuraxial CSF to the periphery has been catalyzed by an implication of reduction in these processes in neurological disease development. Although magnetic resonance imaging (MRI) with ITH Gadolinium-DTPA is beginning to be used to study these processes in humans, this approach lacks quantitative sensitivity and has raised potential safety concerns.
2. Interpretation: We evaluated several pragmatic factors to develop the use of ITH ^{99m}Tc-DTPA imaging for studying the movement of molecule between CSF, CNS, and periphery. Lumbar ITH dosing of this widely available radiopharmaceutical allowed estimations of neuraxial molecular spread, CSF-CNS exchange, and CSF-peripheral clearance.
3. Future directions: Our study provides insights for not only studying brain-CSF molecular clearance processes, but also informs ITH therapeutic dosing efforts that aim to use the lumbar cistern dosing route to deliver drug molecules to the brain. Dosing principles elucidated by our study may also aid the development of other ITH imaging biomarkers.

2 | METHODS

2.1 | Data acquisition

2.1.1 | Human participants

All procedures were approved by the Weill Cornell Medical College Institutional Review Board after an explicit "Approval to Proceed" letter was obtained from the U.S. Food and Drug Administration (FDA). All participants gave informed consent, which was documented in writing. Selection criteria included being subjectively healthy and the absence of any major medical problems by history, on-study physical examination, a set of clinical laboratory studies, and repeated urine drug screens. MR images were used to exclude participants who had any relative contraindications to lumbar puncture or significant spinal stenosis that could impair normal CSF transit. The population included nine males and six females with a mean ± SD age of 38.7 ± 8.1 years (range: 23 to 49). Demographic and biometric information for all subjects was previously reported in a publication describing the use of MRI to calculate CSF volumes (1). Some of these biometric data are

used as statistical covariates in the current work and so are presented again here in Table S1.

2.2 | Radiopharmaceutical

Kits for the preparation of ^{99m}Tc pentatate (DTPA) were acquired commercially (Jubilant Draximage, Quebec, CA, USA). The kit was radiolabeled with freshly eluted ^{99m}Tc pertechnetate (TcO_4^-) in saline. The radiopharmaceutical was then diluted in artificial CSF (aCSF). Current good manufacturing practice was used. All activity preparations were shown to pass quality control specifications for radiochemical purity. All activity preparations were prospectively shown to pass tests of pyrogenicity before administration. Sterility tests were performed post hoc.

2.3 | Imaging and activity quantification

Healthy volunteers were intrathecally administered an activity of 185 ± 14 MBq (5.0 ± 0.4 mCi) of ^{99m}Tc-DTPA in aCSF using Whitacre-style Gertie Marx (International Medical Development, Huntsville, UT, USA) atraumatic spinal needles under fluoroscopic guidance. The injection site was between L2/L3 or L3/L4 for all subjects. The protocol specified that the bolus was to be administered at a rate of 5 mL/minutes. The clinical fluoroscopy suite where the ^{99m}Tc-DTPA injection took place was located in a different part of the hospital than the nucelar imaging facility. This led to some minor variability of ±10 minutes in patient transport time and achieving the targeted time for the first image aquisitions. Starting at about 30 minutes after administration (range: 19 to 34 minutes), 16.6 ± 4.5 (range: 12 to 22) serial whole-body, conjugate planar scintigraphic images were acquired during the first 8 hours after administration, with a final planar acquisition at ≈22 hours after injection. Scans were performed over an ≈ 200 cm field of view on a dual-headed camera (Forte, Philips ADAC, Cincinnati, OH, USA). A 20% energy window was centered on 140 keV. The matrix size was 1024 × 512, with a 2-mm × 2-mm pixel size. Whole-body scans were acquired with either a 6-minute or 12-minute scan duration, except for the last scan at 22 hours, which had a 24-minute scan duration to compensate for radioactive decay. Shortly prior to administration of the radiopharmaceutical, a transmission image was performed for attenuation correction with a Cobalt-57 sheet source using identical acquisition parameters as the emission images. Attenuation corrected geometric means were calculated from conjugate anterior and posterior images. The dynamic, planar images were co-registered to the transmission scans and corrected for acquisition duration, decay, and attenuation. Three-dimensional SPECT/CT scans were performed starting at about 8 and 22 hours after dosing. Each SPECT/CT scan was performed on a dual headed camera (Optima 640; GE Healthcare, Milwaukee, WI, USA). The scans covered two fields of view (FOVs) of 40 cm each starting at the vertex of the skull and extending as far down the neuroaxis as feasible. The acquisition parameters included 60 stops per head in a step-and-shoot mode for a duration of 30 minutes per FOV. Planar transmission and emission scans, as well as 3T MRI scans co-registered to the SPECT scans, were used to place 18 regions of interest, including CSF (lumbar, lower thoracic, upper thoracic, cervical, cisterna magna), brain (substantia nigra, midbrain, motor cortex, frontal, hippocampus, ponto-medullary junction, and remainder), left and right kidneys, bladder, waste bottle, and background. A background region was placed superior to the left shoulder of the participants, and was used to calculate a background scatter correction factor.[21] The activity map for each time point was normalized by the total integrated signal at the earliest time point and multiplied by 100 to create a percentage injected activity map. The earliest time point image available was chosen under the assumption that, because no waste was eliminated by any participant, the integrated activity was representative of the entire administered activity, or 100% of the injected dose.

2.4 | Evaluation of conditions impacting cranial delivery

To optimize rostral neuraxial delivery of lumbar IT dosed ^{99m}Tc-DTPA into the cranium, two means of enhancing CSF convection were tested. All procedures started by aspirating 5 mL of CSF, which was fractionated for analysis by the clinical laboratory and placement in a tissue repository. Then, a net dose of 185 ± 14 MBq of ^{99m}Tc-DTPA was administered by hand over ≈ 5 minutes. The DTPA formulation was diluted in 5, 15, or 30 mL (n = 3 per cohort) of aCSF. Thus, the net positive amount of aCSF added into the SAS was 0, 10, and 25 mL for the respective bolus volume conditions. Two other cohorts (n = 3 each) underwent 5 mL CSF removal and 5 mL bolus injection followed by application of mechanical convective force application to the torso using a high frequency chest wall or lumbothoracic oscillating respiratory clearance device (Smart Vest or Smart Wrap, Electromed Inc, New Prague, MN, USA). The vest covered the shoulders and upper thorax. The wrap was placed around the lumbar and lower thoracic back. Several days before the study, the subjects practiced wearing the devices to ensure tolerance and promote comfort. Both were applied at 50 to 60 Hz depending on subject tolerance for 30 minutes. These maneuvers were intended to enhance mechanical convection well beyond that produced by physiological heartbeats or ventilation. Overall heart rate, ventilation, and physical activity were also monitored in subjects by means of wearable sensors in the form of a Smart Shirt sensor (Hexoskin; Carre Technologies, Inc., Montreal, QC, Canada). All subjects were instructed to limit physical activity to no more than walking about 40 meters from the hospital clinic to the on-campus hospital hotel at the 9 hours post-injection mark. Compliance was verified post hoc by the accelerometer in the Smart Shirt sensor. The impact of inter-individual CSF volume variability was also evaluated by using whole body MRI to assess individual CSF volume and determine volume-based corrections. The MRI measured spinal and cranial volumes from all subjects in this study including the screen failures have been reported previously.[1]

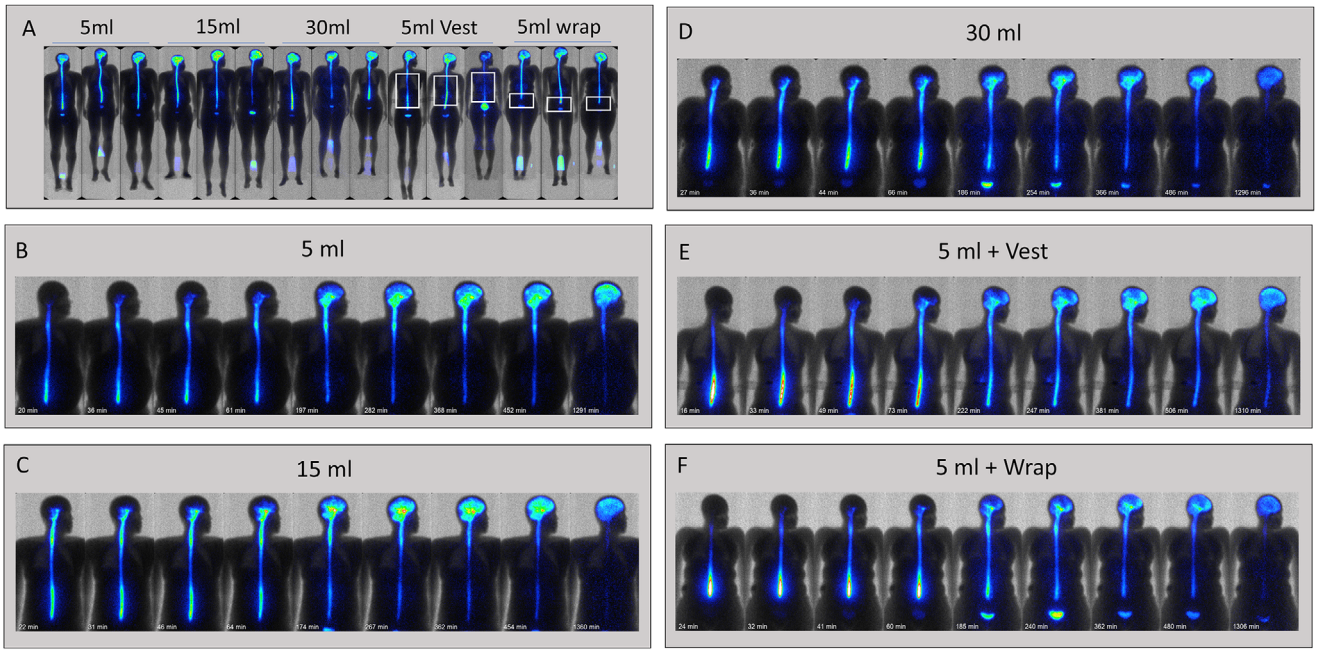

FIGURE 1 Time course of caudat to rostral neuraxial spread of lumbar ITH dosed ^{99m}Tc-DTPA. Following lumbar puncture and removal of 5 mL of CSF, cohorts of three subjects each were dosed ITH with ^{99m}Tc-DTPA formulated in either 5 mL, 15 mL, or 30 mL of aCSF at a rate of 5 mL/minute. An additional two cohorts of two subjects each were dosed with ^{99m}Tc-DTPA in 5 mL aCSF immediately followed by the application of mechanical percussion via an oscillating vest worn over the thorax or an oscillating wrap covering the lumbosacral region (60 Hz, 30 minutes for each). Serial planar scintigraphy images were obtained at the indicated times and overlaid onto a common silhouette for each subject. All images were corrected for decay. Panel A shows planar scintigraphy data overlaid on the body habitus images for all subjects by dosing group at ≈ 8 hours post-dosing. In several examples, signal from the urine collection bottles can be seen in the field of view. The approximate area covered by the mechanical vest or wrap is also outlined. Panels B-F show the time series of ^{99m}Tc-DTPA scintigraphy with the post-dosing image acquisition times indicated under each image

3 | RESULTS

3.1 | Data acquisition

The final sample consisted of nine men and six women with a mean age of 38.7 ± 8.1 years (range: 23 to 49). The findings showed that the safety features built into our study design, the use of non-cutting needles, were effective at reducing adverse events to rates far below those reported in clinical settings.[22,23] There were no medically meaningful adverse events related to the drug formulation. Lateral planar images at the 60-minute after-injection mark as well as SPECT images at the 8- and 22-hour marks showed that there were no abnormal extraspinal activity outside the ITH spaces. Follow-up at 48 hours and 1-week post-administration showed that no subjects developed a post-LP headache syndrome. Subjects in the mechanical oscillation groups wore the devices during all emission and transmission scans, even when it was not turned on.

3.2 | Cranial delivery optimization

The lumbar CSF cistern provides the most convenient access to the SAS. However, reliable means for rostral molecular movement are needed to ensure reaching the cranium from the lumbar region. Neuraxial spread of molecules placed into the lumbar ITH space may be influenced by individual body habitus, CSF volumes, and convective forces from the injection procedures, or mechanical forces impacting on the SAS including pulsatile heart contractions, ventilation, and physical activity.[2-5] These factors were evaluated for their effect on timing of cranial ^{99m}Tc-DTPA delivery.

Planar images demonstrating body habitus variability among the study subjects for each dosing group are shown in Figure 1A along with scintigraphy images taken at ≈8 hours post-dosing. The images show ^{99m}Tc-DTPA signal in the neuraxis, bladder, and urine collection bottles placed in the field of view. The approximate placement of the mechanical oscillation vest or wrap for the respective cohorts are also indicated in Figure 1A. Individual examples of the imaging time-course from each dosing condition group are shown in Figure 1B–F. Lumbar ITH dosing of ^{99m}Tc-DTPA led to sequential rostral movement of signal from the lumbar to the thoracic, cervical, and cranial regions. Between 3 and 8 hours, the relative cranial ^{99m}Tc-DTPA signal was observed to increase, and by the last imaging time point neuraxial signal distribution was highest in the brain (Figure 1B–F). Despite some inter-subject variability, the relative rate of cranial signal appearance and overall exposure (area under the curve [AUC]) following lumbar ITH dosing trended to be higher with the 15 mL bolus volume as compared with the 5 mL bolus volume. Tables 1 and 2 show the percentage of injected activity detected in the lumbar and cranial

TABLE 1 Lumbar and cranial time course of 99mTc-DTPA signal (percentage of injected activity)

Group		1 Hour	4 Hours	20 Hours
5 mL	Lumbar	52.7 ± 7.9†	24.2 ± 8.6	5.7 ± 1.9
	Cranial	2.5 ± 2.7†	22.9 ± 12.2	33.5 ± 10.2
15 m	Lumbar	29.6 ± 2.7	9.0 ± 2.0	1.8 ± 0.8†
	Cranial	13.2 ± 5.2	37.7 ± 6.6	29.9 ± 4.0
30 mL	Lumbar	46.2 ± 11.4	20.6 ± 8.4	4.2 ± 2.3
	Cranial	8.6 ± 4.7	24.0 ± 5.8	24.8 ± 9.8
5 mL Vest	Lumbar	46.8 ± 7.8†	20.8 ± 11.9	4.3 ± 4.1
	Cranial	2.2 ± 2.2†	14.0 ± 8.8†	18.1 ± 14.4
5 mL Wrap	Lumbar	47.6 ± 7.1†	15.7 ± 3.4†	2.5 ± 1.3
	Cranial	9.8 ± 8.4	29.6 ± 14.5	22.3 ± 7.0

Time course of lumbar and cranial ^{99m}Tc-DTPA signal for each dosing group. Data are presented as percentage of injected activity measured at 1, 4, and 20 hours (mean ± SEM; n = 3). All subjects were imaged within 11% of the indicated post-dosing time. Asterisks indicate statistically significant differences from the 5 mL alone condition.

ITH compartments at 1, 4, and 20 hours post-dosing for each dosing condition. At the 1-hour timepoint, the percentage of injected activity was greater in cranium and lower in the lumbar region for the 15 mL group compared to all other groups. This difference was statistically significant ($P < 0.05$, two-tailed, independent sample t test) for two and three of the four comparator groups in the cranium and lumbar compartments, respectively. The same trend was observed 4 hours post-administration and is statistically significant for one each of the four comparator groups in the cranium and lumbar compartment, respectively.

Further enhancement of convection by increasing the bolus volume to 30 mL did not produce greater cranial translocation of ^{99m}Tc-DTPA signal. Instead this appeared to increase peripheral elimination. Mechanical oscillation also did not further enhance cranial delivery of signal as compared to the 5 mL bolus condition alone (Figure 1, Tables 1 and 2). In fact, the 5 mL + Vest cohort trended to display a lower percentage of injected activity in the cranium as compared to the 5 or 15 mL groups. When measured over the full ≈22 hours, a lower lumbar but higher cranial ^{99m}Tc-DTPA exposure (AUC) was seen in the 15 mL group than the 5 mL group. This differential pattern was maintained upon correction for MRI-derived individual lumbar and cranial CSF volumes (Table 2).

TABLE 3 99mTc-DTPA urinary excretion

	5 mL	15 mL	30 mL	5 mL vest	5 mL wrap
6 hours	9.6%	14.0%	14.4%	22.5%	7.8%
22 hours	26.8%	29.5%	36.0%	47.9%	33.8%

Urinary excretion of ITH ^{99m}Tc-DTPA. Urine was collected in all subjects over time. The accumulated urinary ^{99m}Tc-DTPA signals measured by scintigraphy is displayed as the mean value of percentage injected dose measured from each dosing group (n = 3) for the first 6 hours and for the entire study period. Reported values were corrected for total CSF volume.

3.3 | Clearance from CSF to periphery

Individual examples of the change in relative neuraxial planar SPECT signal over time for each dosing condition are displayed as videos in Supplementary Video 1. These data show the periodic accumulation of signal in the bladder, followed by urinary voiding into collection bottles (Supplementary Video 1). Subjects provided a mean ± SD of 12.5 ± 3.5 (range: 10 to 18) discrete urine samples over 6 hours, and 16.6 ± 4.5 (range: 13 to 24) discrete urine samples over 22 hours. After background scatter correction and individual CSF total volume correction, conjugate imaging showed a linear relationship between increased urinary clearance of the percentage injected dose with the volume of infusate, and even greater excretion with both of the high frequency oscillation conditions (Table 3). An evaluation of ITH and peripheral tissue exposure showed the mean ITH residence time for of ^{99m}Tc-DTPA to be >6 hours for all conditions, suggesting that clearance to the periphery was a slow process.

Graphical analysis of the data in Tables 1 and 3 suggested that unlike the 15 mL group, the 30 mL and 5 mL + mechanical oscillation conditions did not boost percentage injected activity or AUC of ^{99m}Tc-DTPA to the cranial compartment over the 5 mL group (Figure 2A). Instead, an enhancement of clearance to the periphery was induced by the higher volume (30 mL) and oscillation conditions, being most prominent for the Vest condition (Figure 2A). Enhancement of paraspinal ^{99m}Tc-DTPA scintigraphy signal was observed in the 30-mL and mechanical oscillation groups, with an anatomical pattern resembling lumbar spinal nerve roots, which has been proposed to mediate CSF clearance from the SAS via the PCOP.[19,20] As with the suggestion of reduced cranial delivery and increase urinary clearance, this imaging pattern was most prominent for the high frequency oscillation dosing conditions (Figure 2B).

TABLE 2 Lumbar and cranial 99mTc-DTPA exposure (AUC)

Group	Lumbar CSF AUC (h)	Cranial CSF AUC (h)	Lumbar normalized CSF AUC (h/L)	Cranial normalized CSF AUC (h/L)
5 mL	2.03 ± 0.49	2.15 ± 0.96	7.8 ± 2.5	8.2 ± 3.1
15 mL	0.91 ± 0.17	3.04 ± 0.26	3.8 ± 0.4	12.9 ± 2.7
30 mL	1.84 ± 0.69	2.08 ± 0.60	5.8 ± 2.8	6.4 ± 1.7
5 mL with Vest	1.89 ± 0.81	1.37 ± 0.99	9.0 ± 7.4	6.4 ± 5.7
5 mL with Wrap	1.53 ± 0.13	2.37 ± 1.18	6.7 ± 1.4	9.8 ± 3.2

Overall ^{99m}Tc-DTPA exposure (area under the curve; AUC) of the lumbar and cranial neuraxial compartments for each dosing group.

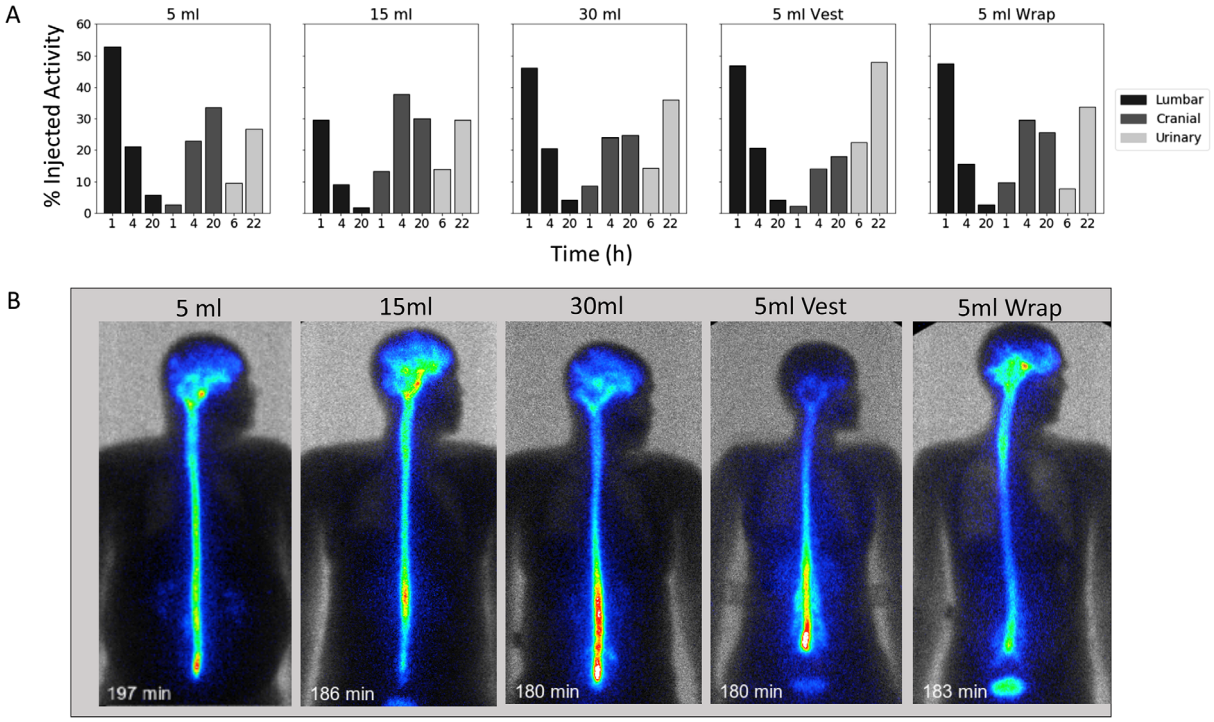

FIGURE 2 Relative temporal cranial versus lumbar CSF signal per dosing group. (A) Percentage injected activity in the lumbar versus cranial region is plotted at 1 hour, 4 hours, and 20 hours for each dosing group. Percentage injected activity accumulated in urine over 6 hours and 22 hours is also displayed. (B) Individual examples of ^{99m}Tc-DTPA planar imaging at ≈ 3 hours following lumbar ITH dosing. Higher lumbar, paraspinal, and nerve root signal enhancement was observed with the 30 mL and mechanical convection conditions. The lower edge of the oscillatory vest can be seen in the silhouette image from that group

3.4 | Assessment of brain ISF penetration

Anatomical assessment of brain penetration of lumbar ITH dosed ^{99m}Tc-DTPA was performed via two-dimensional (2D) and 3D analyses of SPECT-CT scans taken at 8 and 22 hours post-dosing. At these time points all subjects showed presence of cranial signal by planar scintigraphy. Figure 3 displays 3D and 2D SPECT CT data from a subject given a 15-mL volume dose. Centripetal cranial signal translocation from the CSF cisterns into CNS tissue lying adjacent to the SAS appeared to take place earlier in the 15-mL group than in other groups. ^{99m}Tc-DTPA signal was clearly seen to enter the cerebellar and cerebral cortices uniformly, while deep brain structures such at the striatum, thalamus, and deep cerebellar nuclei showed little signal accumulation over the studied timepoints. A 3D movie display of these data is shown in Supplemental Video 2. Nearly all signal detected in the cranium at the 22-hour timepoint was associated with the brain and spinal cord parenchyma. A quantitative assessment was performed using planar scintigraphy data. Examples of the regions of interest (ROIs) used are shown in Figure S1 and quantitative output is available in Table S2

4 | DISCUSSION

This pilot study investigated the feasibility of using ^{99m}Tc-DTPA to evaluate molecular exchange dynamics between the CSF, CNS, and periphery. Decreased clearance of toxic proteins from brain into the CSF in subjects with several neurodegenerative diseases has implicated faulty brain-CSF-periphery exchange mechanisms in contributing to the pathophysiology of neurodegenerative and neuroimmune disorders.[6-12,24] This physiology has been studied in animals over many decades by tracking the kinetics of injected probes from brain to CSF and from CSF to brain, and the clinical feasibility of this approach also has been established using ITH Gd-DTPA dosing with MRI assessment.[14,15] However, given the millimolar concentrations of Gd-DTPA required for MRI imaging and the concern over potentially toxic CNS Gd retention, this method remains sub-optimal for routine clinical application.[16] In contrast, ^{99m}Tc-DTPA is a highly stable radiometal chelate that has long been used safely in clinical ITH imaging to localize sites of CSF leaks following trauma or in chronic headache settings.[17] Given the much lower doses required, high radioactive sensitivity, and 6-hour radiolabel half-life of ^{99m}Tc-DTPA, ITH planar scintigraphy or SPECT imaging with this widely available imaging probe and modality may be more appropriate for routine assessment of molecular exchange between CSF, CNS, and periphery.

We used ITH lumbar cistern dosing to assess the ability of ^{99m}Tc-DTPA to visualize neuraxial molecular pharmacokinetics, CSF-brain molecular exchange, and CSF-peripheral clearance. Because dosing via lumbar puncture can lead to significant caudal to rostral molecular gradients,[4,5] we evaluated the effect of CSF convection–enhancing approaches on cranial entry of lumbar ITH dosed ^{99m}Tc-DTPA in

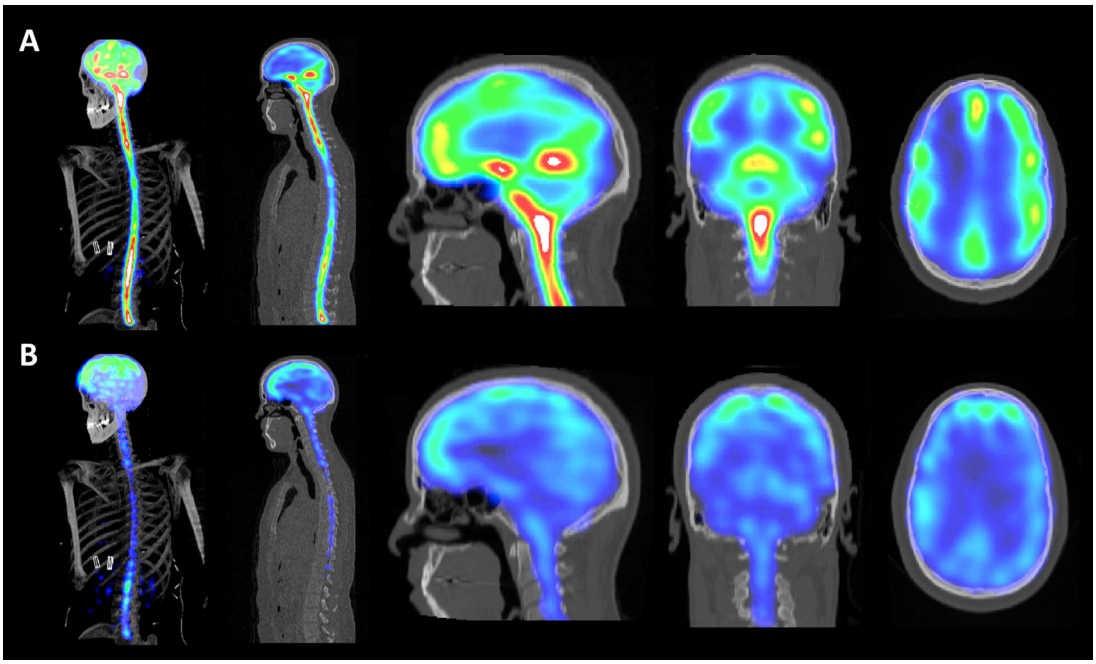

FIGURE 3 3D and 2D imaging of brain translocation of ^{99m}TC-DTPA signal. Example images are from a subject dosed with ^{99m}TC-DTPA formulated in 15 mL aCSF. Panels A and B show ^{99m}TC-DTPA images at 8 hours and 22 hours post-dosing, respectively. From left to right, the figures depict 3D SPECT CT MIP images followed by 2D SPECT sagittal images of the whole neuraxis as well as 2D SPECT CT sagittal, coronal, and horizontal images of the head. The imaging scale was adjusted to show serial translocation of relative ^{99m}TC-DTPA signal into cortical structures between the two time points

normal human volunteers. Despite the small number of subjects in our study, we demonstrated cranial signal entry following LP dosing and apparent CNS ISF uptake in every subject. Use of atraumatic needles as well as dosing an equal or greater volume of the aCSF ^{99m}Tc-DTPA formulation, as compared to the 5-mL CSF removal, led to high tolerability with no headaches reported. Although the 5-mL dosing volume gave adequate cranial and brain signal by 8 and 22 hours, the 15-mL dose appeared to give a more uniform and strong earlier cranial and brain signal. Surprisingly, a higher dosing volume of 30 mL, or application of external mechanical force using either thoracic or lumbar percussion, did not improve cranial translocation of signal over the 5- or 15 mL dose. In fact, the higher convective stimuli trended toward greater urinary excretion. The PCOP has been described previously as a clearance path for CSF along nerve root sheaths[19] and may encompass both egress via true lymphatic vessels located in the dural meninges and nerve root sheaths as well as arachnoid granulations. We speculate that a combination of pressure and volume effects in the lumbar cistern arising from the higher convective stimuli aided in the peripheral clearance of ITH dosed ^{99m}Tc-DTPA via the above-envisioned routes. The oscillating vest utilized in our study is used for clearing respiratory airways in children with disorders such as with cystic fibrosis and spinal muscular atrophy. In our adult subjects, this oscillating vest did not fully cover the neuraxis (Figure 1A). Positioning of the vest above the lumbar region may have enhanced radiotracer egress through lumbar nerve root PCOP routes, as suggested by an increase in the lumbar paraspinal enhancement imaging pattern (Figure 2B). The delayed appearance of urinary signal suggests a more prominent role for the slower transit meningeal and nerve root lymphatics as compared to arachnoid granulations. Meningeal and nerve root lymphatics have long been demonstrated in many mammalian species and have recently regained significant revival of interest for their potential role CSF clearance and neuroimmune surveillance.[25-28]

Because DTPA chelates do not readily enter cells, we assume that the observed movement of ^{99m}Tc-DTPA from the SAS into the brain parenchyma represents entry into brain ISF. Cerebral cortical structures clearly showed ^{99m}Tc-DTPA signal accumulation but deeper structures such as basal ganglia and thalamus showed little uptake (Figure 3, Table S1). These observations are consistent with ITH imaging studies using Gd-DTPA.[13-15] However, ^{99m}Tc-DTPA scintigraphy allowed quantitative assessment of the low amounts of molecular exchange between the CSF and cerebral cortex by 22 hours post-dosing, with the SPECT CT imaging demonstrating brain association of the radioactive signal (Figure S1 and Table S1). It is likely that a portion of the peripherally cleared signal also represents efflux of ^{99m}Tc-DTPA from the CNS ISF across the BBB, and the methods used here cannot resolve this process. We did observe some regional heterogeneity in signal uptake between cerebral cortical regions, and it is not yet clear whether this represents inherent regional brain differences in human brain CSF-ISF exchange or differences in relative regional ^{99m}Tc-DTPA delivery achieved by our delivery methods.

Sleep stage–related changes in CSF volume, turnover, and exchange with ISF have also been suggested by recent human studies.[29,30] Given the long duration of our overall serial imaging study, subjects were allowed maintain their usual circadian sleep cycles in the on-campus

hotel the night before, and the first night after the dosing procedure. Thus, we cannot rule out the effects of sleep on our measurements. The relative ease and patient comfort of planar scintigraphy and SPECT scanning does afford the future opportunity to measure changes in cortical ^{99m}Tc-DTPA signal accumulation and retention during sleep stages or upon exposure to drugs. ITH ^{99m}Tc-DTPA imaging may also be useful in several disorders spanning cortical dementias, strokes, trauma, and autoimmune disease to help clarify a role for CSF-brain molecular exchange alterations in these conditions. Further work in larger numbers of both normal subjects and patient populations is needed to develop these applications.

5 | CONCLUSION

This pilot study explored the pragmatic expansion of ITH ^{99m}Tc-DTPA imaging applications beyond its use in assessment of traumatic CSF leaks. ITH ^{99m}Tc-DTPA imaging can be used in clinical research and medical practice for assessing molecular exchange between the CSF, CNS, and periphery in many neurological disorders. Our evaluation of factors impacting neuraxial ^{99m}Tc-DTPA pharmacokinetics can also guide ITH drug dosing practice and future efforts to develop other ITH imaging biomarkers.

ACKNOWLEDGMENTS

This research was funded by Biogen. A.V. was an employee of Biogen at the time of the study.

CONFLICTS OF INTEREST

Ajay Verma was an employee of Biogen during the conduct of this this study. All other authors do not have any conflict of interest to report.

REFERENCES

1. Chazen JL, Dyke JP, Holt RW, et al. Automated segmentation of MR imaging to determine normative central nervous system cerebrospinal fluid volumes in healthy volunteers. *Clinical Imaging*. 2017;43: 132–135. https://doi.org/10.1016/j.clinimag.2017.02.007.
2. Dynamics of respiratory and cardiac CSF motion revealed with real-time simultaneous multi-slice EPI velocity phase contrast imaging. *NeuroImage*. 2015;122: 281–287. https://doi.org/10.1016/j.neuroimage.2015.07.073.
3. Wolf DA, Hesterman JY., Sullivan JM., Orcutt KD., Silva MD, et al. Dynamic dual-isotope molecular imaging elucidates principles for optimizing intrathecal drug delivery. *JCI Insight*. 2016;1: 2:https://doi.org/10.1172/jci.insight.85311.
4. Mazur C, Powers B, Zasadny K, et al. Brain pharmacology of intrathecal antisense oligonucleotides revealed through multimodal imaging. *JCI Insight*. 2019;4(20):e129240. https://doi.org/10.1172/jci.insight.129240.
5. Papisov MI, Belov VV, Gannon KS. Physiology of the intrathecal bolus: the leptomeningeal route for macromolecule and particle delivery to CNS. *Mol Pharm*. 2013;10(5):1522-1532. https://doi.org/10.1021/mp300474m.
6. Bakker EN, Bacskai BJ, Arbel-Ornath M, et al. Lymphatic clearance of the brain: perivascular, paravascular and significance for neurodegenerative diseases. *Cell Mol Neurobiol*. 2016;36(2):181-194. https://doi.org/10.1007/s10571-015-0273-8.
7. Engelhardt B, Vaikoczy P, Weller RO. The movers and shapers in immune privilege of the CNS. *Nat Immunol*. 2017;18(2):123-131. https://doi.org/10.1038/ni.3666.
8. Benveniste H, Liu X, Koundal S, Sanggaard S, Lee H, Wardlaw J. The glymphatic system and waste clearance with brain aging: a review. *Gerontology*. 2019;65:106-119. https://doi.org/10.1159/000490349.
9. Sullan MJ, Asken BM, Jaffee MS, DeKosky ST, Bauer RM. Glymphatic system disruption as a mediator of brain trauma and chronic traumatic encephalopathy. *Neurosci Biobehav Rev*. 2018;84:316-324. https://doi.org/10.1016/j.neubiorev.2017.08.016.
10. Mawuenyega KG, Sigrudson W, Ovod V, et al. Decreased clearance of CNS beta-amyloid in Alzheimer's disease. *Science*. 2010;330(6012):1774. https://doi.org/10.1126/science.1197623.
11. Iliff JJ, Wang M, Liao Y, et al. A paravascular pathway facilitates CSF flow through the brain parenchyma and the clearance of interstitial solutes, including amyloid beta. *Sci Transl Med*. 2012;4(147):147ra111. https://doi.org/10.1126/scitranslmed.3003748.
12. Iliff JJ, Lee H, Yu M, et al. Brain-wide pathway for waste clearance captured by contrast-enhanced MRI. *J Clin Invest*. 2013;123(3):1299-1309. https://doi.org/10.1172/JCI67677.
13. Jinkins JR, Williams RF, Xiong L. Evaluation of gadopentetate dimeglumine magnetic resonance cisternography in an animal model. *Invest Radiol*. 1999;349(2):156-159. https://doi.org/10.1097/00004424-199902000-00009.
14. Ringstad G, Valnes LM, Dale AM, et al. Brain-wide glymphatic enhancement and clearance in humans assessed with MRI. *JCI Insight*. 2018;;3(13):pii:121537. https://doi.org/10.1172/jci.insight.121537.
15. Eide PK, Vatnehol SAS, Emblem KE, Ringstad G. Magnetic resonance imaging provides evidence of glymphatic drainage from human brain to cervical lymph nodes. *Sci Rep*. 2018;8(1):7194. https://doi.org/10.1038/s41598-018-25666-4.
16. Hagedorn JM, Bendel MA, Moeschler SM, Lamer TJ, Pope JE, Deer TR. Intrathecal gadolinium use for the chronic pain physician. *Neuromodulation*. 2019;22(7):769-774. https://doi.org/10.1111/ner.13043.
17. Novotny C, Potzi C, Asenbaum S, Peloschek K, Suess E, Hoffmann M. SPECT/CT fusion imaging in radionuclide cisternography for localization of liquor leakage sites.. *J Neuroimaging*. 2009;;19(3):227–234.. https://doi.org/10.1111/j.1552-6569.2008.00270.
18. Hesterman J, Kost S, Holt R, Dobson H, Verma A, Mozley PD. Three-dimensional dosimetry for radiation safety estimates from intrathecal administration. *J Nucl Med*. 2017;58(10):1672-1678. https://doi.org/10.2967/jnumed.117.190611.
19. Bechter K, Schmitz B. Cerebrospinal fluid outflow along lumbar nerves and possible relevance for pain research: case report and review. *Croat Med J*. 2014;55(4):399-404. Review. https://doi.org/10.3325/cmj.2014.55.399.
20. Schmitt M, Neubauer A, Greiner J, Xu X, Barth TF, Bechter K. Spreading of acute myeloid leukemia cells by trafficking along the peripheral outflow pathway of cerebrospinal fluid. *Anticancer Res*. 2011;31(6):2343-2345.
21. Mozley PD, Stubbs JB, Kim H-J, McElgin W, Kung HF. Biodistribution and dosimetry of iodine-123-labeled tropane to image dopamine transporters. *J Nucl Med*. 1996;371::151-159.
22. Byrnes DM, Vargas F, Dermarkarian C, et al. Complications of intrathecal chemotherapy in adults: single-institution experience in 109 consecutive patients. *J Oncol*. 2019;2019:4047617. https://doi.org/10.1155/2019/4047617.
23. Batova R, Georgiev S. Impact of spinal needle design and approach to postdural puncture headache and spinal anesthesia failure in obstetrics. *Anaesthesiol Intensive Ther*. 2019;51:77-82. https://doi.org/10.5114/ait.2019.86166.
24. Tarasoff-Conway JM, Carare RO, Osorio RS, et al. Clearance systems in the brain-implications for Alzheimer disease. *Nat Rev Neurol*. 2015;11(8):457-470. https://doi.org/10.1038/nrneurol.2015.119.

25. Zenker W, Bankoul S, Braun JS. Morphological indications for considerable diffuse reabsorption of cerebrospinal fluid in spinal meninges particularly in the areas of meningeal funnels. An electronmicroscopical study including tracing experiments in rats. *Anat Embryol*. 1994;189(3):243-258. https://doi.org/10.1007/bf00239012.
26. Ma Q, Decker Y, Müller A, Ineichen BV, Proulx ST. Clearance of cerebrospinal fluid from the sacral spine through lymphatic vessels. *J Exp Med*. 2019;216(11):2492-2502. https://doi.org/10.1084/jem.20190351.
27. Miura M, Kato S, vonLüdinghausen M. Lymphatic drainage of the cerebrospinal fluid from monkey spinal meninges with special reference to the distribution of the epidural lymphatics. *Arch Histol Cytol*. 1998;61(3):277-286. https://doi.org/10.1679/aohc.61.277.
28. Jacob L, Boisserand LSB, Geraldo LHM, et al. Anatomy and function of the vertebral column lymphatic network in mice. *Nat Commun*. 2019;10(1):4594. https://doi.org/10.1038/s41467-019-12568-w.
29. Meghdadi AH, Popovic D, Rupp G, Smith S, Berka C, Verma A. Transcranial impedance changes during sleep: a rheoencephalography study. *IEEE J Transl Eng Health Med*. 2019;7:2700107. https://doi.org/10.1109/JTEHM.2019.2898193.
30. Fultz NE, Bonmassar G, Setsompop K, et al. Coupled electrophysiological, hemodynamic, and cerebrospinal fluid oscillations in human sleep. *Science*. 2019;366(6465):628-631. https://doi.org/10.1126/science.aax5440.

SUPPORTING INFORMATION

Additional supporting information may be found online in the Supporting Information section at the end of the article.

How to cite this article: Verma A, Hesterman JY, Chazen JL, et al. Intrathecal ^{99m}Tc-DTPA imaging of molecular passage from lumbar cerebrospinal fluid to brain and periphery in humans. *Alzheimer's Dement*. 2020;12:e12030. https://doi.org/10.1002/dad2.12030